# Synthesis and Properties of Monolayer Protected $Co_x(SC_2H_4Ph)_m$ Nanoclusters

*Stephan Pollitt[1], Ernst Pittenauer[2], Christoph Rameshan[1], Thomas Schachinger[3], Olga V. Safonova[4], Vera Truttmann[1], Abhijit Bera[1], Günter Allmaier[2], Noelia Barrabés[1*], Günther Rupprechter[1]*

[1] Institute of Materials Chemistry, Technische Universität Wien, Getreidemarkt 9/165, 1060, Vienna, Austria

[2]Institute of Chemical Technologies and Analytics, Technische Universität Wien, Getreidemarkt 9/164, 1060, Vienna, Austria

[3] University Service Centre for Transmission Electron Microscopy (USTEM), Technische Universität Wien, Wiedner Hauptstraße 8-10, 1040 Vienna, Austria

[4]Paul Scherrer Institute, 5232 Villigen PSI, Switzerland

ABSTRACT

Nanometer-sized and stable thiolate-protected cobalt clusters were synthesized by a wet chemical method, leading to a pink solution with well-defined optical activity (UV-Vis) and photoluminescence (PL). The cobalt cluster core of ~1.3 nm size was metallic (as indicated by STEM, STM, XPS, HAADF-EELS) and was surrounded by a specific configuration of thiolate

staples (according to Raman, FTIR, XAFS, MALDI) that is similar to that of corresponding gold clusters.

## INTRODUCTION

Metal nanoclusters with less than 100 atoms have recently become an intensively studied field, due to their size-dependent properties, which do not follow the common scaling laws of bulk materials. Their unique atomic structures lead to different quantized electronic states, redox-, photoluminescent-, magnetic and catalytic properties.[1-4] This points to a variety of potential applications in sensor technology[5-6], biomedical applications,[7] nanoelectronics and catalysis.[1, 8-9]

Significant previous research activities during the last decade have focused on thiolate protected Au and Ag clusters, including optimization of different atomic sizes, composition (bi-, tri-metallic clusters), and structure, revealing exciting properties at the nanoscale.[1] However, metal nanoclusters other than gold or silver have rarely been studied, due to difficulties in successfully synthesizing stable structures in the range of a few atoms. Recently, new metal clusters such as $Ni_x(SC_2H_4Ph)_m$ (x=6,39,41)[10-12], $Cu_{38}(SC_2H_4Ph)_{25}$, [13] or $Ir_9(SC_2H_4Ph)_6$[14] have been reported , showing enhanced properties when compared with the pure metal nanoparticles.

Cobalt (Co) is a metal with loosely bonded *d* electrons and also exhibits size-dependent structural, magnetic, electronic and catalytic properties. The exponential dependence of the magnetization relaxation time on volume has stimulated intensive studies of Co nanocrystal synthesis for magnetic storage applications.[15] However, unlike gold or silver, zero-valent cobalt nanometal is very sensitive to air, creating a challenge to stabilize cobalt nanoparticles in different media. A few preceding studies have shown that via passivation by organic thiols the oxidation and agglomeration of metallic Co particles can be avoided, leading to particles in the micron size.[16-17]

In addition, several recent studies have focused on the synthesis of defined cobalt sulfide ($CoS_2$) nanostructures. Cobalt sulfides have phase-dependent electronic, magnetic and catalytic properties, opening potential applications in energy conversion and storage. Due the low over potential, high durability and good cyclability, $CoS_2$ may also be used in batteries. $CoS_2$ also showed high capacitance in electrochemical capacitors, due to its high redox activity, for example in dye-sensitized solar cells. High efficiency of $CoS_2$ has been also observed in hydrogen evolution electrocatalysis[18-19] and photoelectrochemical[20] processes.[21-23] Thus, thiolated cobalt nanoclusters may represent an interesting approach towards well-defined cobalt sulfide nanostructures, with great potential in several applications.

As mentioned, cobalt exhibits loosely bonded d-electrons and high electrical conductivity, which makes it suitable for catalytic applications both in metallic and oxidic form. Obtaining truly homogeneous and well-defined nanostructures is very beneficial for understanding catalytic reaction mechanisms on an atomic level, since it typically depends on nanoparticle size and structure. For example, when cobalt oxides were grown from colloidal cobalt particles of defined size, better insights into their CO oxidation activity were obtained.[24] Colloidal particles are not structure-resolved, so that cobalt nanoclusters with defined structure could be a better precursor for growing structurally well-defined cobalt oxides.

Consequently, the successful synthesis of cobalt nanostructures would be very rewarding, enabling a broad range of applications in catalytic, photo-, and electrochemical processes. Herein we report the first synthesis of monolayer protected thiolated cobalt clusters in the nanoscale range. The clusters exhibit characteristic UV-Vis spectra and optical properties. The staple configuration of –S-metal-S-, typical of thiolated gold clusters, was also observed in the case of the cobalt clusters, maintaining the cobalt atoms in the metallic state.

## EXPERIMENTAL

### Synthesis

The synthesis of $Co_x(SR)_m$ clusters follows a modified Brust[25] method. $Co_2Cl{\cdot}6H_2O$ (30mg) was dehydrated at 150C in order to be able to be dissolved in terahydrofuran (10mL) upon stirring at room temperature. $PhC_2H_4SH$（0.1mL）was added to the solution and stirred for 30min at room temperature with a change of color from blue to dark blue. An aqueous solution of $NaBH_4$ (80g, 2 mL) cooled to 0 °C was then added at once to the mixture and stirred for 1 h. The reaction mixture was filtered and washed with methanol to remove $PhC_2H_4SH$ and other byproducts. The products were dissolved in methylene chloride leading to a pink solution.

### Co cluster characterization

UV−Vis spectra were recorded on a UV/VIS spectrometer (Perkin Elmer 750 Lambda). Quartz cuvettes of 10 or 5 mm path length were used (solvents: dichloromethane and toluene).

All MALDI mass spectrometric measurements were performed using a prototype Axima $TOF^2$ MALDI time-of-flight (TOF)/reflectron (RTOF) mass spectrometer (Shimadzu, Kratos Analytical). For analytical experiments 2, 4, 6-trihydroxyacetophenone (Sigma-Aldrich) was selected as MALDI-MS matrix. MALDI RTOF mass spectra of the cobalt clusters were acquired near threshold laser irradiance to obtain mass spectra of sufficient mass spectrometric resolution (3000 to 5000 at full width half maximum (FWHM)). All displayed mass spectra were based on averaging 300 to 600 single and unselected laser pulses ($\lambda$ = 337 nm at 50 Hz).

The X-ray powder diffraction measurements were carried out with a Panalytical X'Pert diffractometer in Bragg–Brentano geometry by using Cu-K$\alpha$1,2 radiation, a X-Celerator linear

detector with a Ni filter, sample spinning with back loading sample holders, and 2θ= 5–70° at T = 297 K.

High resolution transmission electron microscopy (HRTEM), high-angle annular dark-field (HAADF) imaging, as well as electron-energy loss spectroscopy (EELS) mapping and energy-dispersive X-ray spectroscopy (EDXS) were performed using a 200 kV FEI TECNAI F20 S-TWIN analytical (scanning) transmission electron microscope (S)TEM equipped with a Gatan GIF Tridiem filter. The energy resolution was ~1 eV, the semi-convergence angle was ~8 mrad, the semi-collection angle was ~15 mrad and the spatial resolution was of the order of 0.5 nm.

Scanning Tunneling Microscopy (STM) images of the nanoclusters were acquired with an Aarhus 150 STM from SPECS. A solution of the clusters was drop-casted on highly ordered pyrolytic graphite (HOPG) as support material. The solvent was evaporated by inserting the sample into the load lock chamber and applying vacuum for 4 hr. The HOPG with the nanoclusters was then transferred to the STM. The base pressure in the STM chamber was $2.2 \times 10^{-10}$ mbar and the clusters were imaged with a Pt/Ir tip at 300 K. During approach of the tip, a current of 0.35 nA and a tunneling voltage of 1.6 V was applied. For image processing and line profile measurement the WSxM software was used.

The Raman microscope system (Renishaw, System 2000; Yobin Yvon, LabRAM HR) consisted of a light microscope (Leica DL-LM; Olympus BX) coupled to a Raman spectrometer. The excitation laser was an Ar ion laser ($k_0$ = 514 nm, source power 17 mW).

X-ray photoelectron spectroscopy (XPS) measurements were performed on a UHV system equipped with a Phoibos 100 hemispherical analyzer and a XR 50 X-ray source (all parts from SPECS GmbH). Spectra were recorded with AlKα radiation and data were analyzed with the CasaXPS software. Peaks were fitted after Shirley background subtraction with Gauss−Lorentz

sum functions. Peak positions and full width at half-maximum (FWHM) were left unconstrained. For the S2p peak fitting doublets with a fixed doublet separation of 1.2 eV (NIST XPS database) and a fixed area ratio of 2:1 were used for $S2p_{3/2}$ and $S2p_{1/2}$. For the XPS measurements the clusters were drop-casted on a highly oriented pyrolytic graphite (HOPG) substrate. This also allowed referencing the binding energies to the C1s signal of HOPG.

X-ray absorption spectroscopy (XAS) measurements were carried out at the XAS beamline at Elettra-Sincrotrone Trieste (Italy) and at the SuperXAS beamline at the Swiss Light Source (Switzerland). S K-edge (2472 eV) was measured at Elettra-Sincrotrone using a Si (111) double-crystal monochromator. The photon flux was about $10^9$ photons/s. Experiments were performed in fluorescence mode using a silicon drift detector (Oxford Instruments). A concentrated solution of the sample was drop-casted on onto sulfur-free polyimide (Kapton) tape and mounted on an in-house made cell working under high vacuum and at liquid nitrogen temperature. XANES at Co K-edge (7709 eV) was measured at Swiss Light Source. The incident photon beam provided by a 2.9 T Super Bend magnet was selected by a Si (111) channel-cut monochromator. The rejection of higher harmonics and focusing were achieved by a Si-coated collimating mirror at 2.8 mrad and a rhodium-coated toroidal mirror at 2.8 mrad. The size of the X-ray beam on the sample was 0.3 x 0.3 mm with a total intensity of about $5\text{-}7\times10^{11}$ ph/s. Fluorescence signal was detected with five-element SDD detector (SGX). A concentrated solution of the sample in toluene was place in a quartz capillary and cooled down with a cryo-gun to liquid nitrogen temperature. The data analysis was performed according to standard procedures using Ifeffit software. [26]

**RESULTS and DISCUSSION**

**Synthesis of $Co_x(SR)_m$ clusters.** The synthesis strategy of the thiolated cobalt clusters was based on previous synthesis routes of monometallic and bimetallic thiolated gold clusters. However, in light of the comparably easier oxidation of cobalt and, thus, the difficulty to synthesize stable metallic cobalt clusters with a narrow range of particle size, several optimization steps had to be applied. TOAB (tetraoctylammonium bromide), which acts as phase-transfer catalyst, is commonly used in the synthesis of thiolate gold clusters $Au_n(SR)_m$. It improves the solubility of metal salts in organic solvents, which facilitates the reaction. Nevertheless, this kind of quaternary ammonia compounds has a high tendency to oxidize cobalt, which makes the synthesis of metallic cobalt clusters difficult. Thus, TOAB was not used for synthesis and, instead, the hydrated metal salt precursor was dried, which also improved the solubility in THF. The cobalt then forms a complex with THF, which is replaced by the thiolate ligands via a ligand exchange reaction.[27] Since the formation of this starting complex is only possible with $Co^{2+}$, the (further) oxidation of cobalt should be avoided. Thus, for cobalt cluster synthesis short reaction times are beneficial to obtain higher yield of metallic Co. This is due to the tendency of THF to form peroxides that on the one hand are radical starters but on the other hand oxidize cobalt. In contrast, for the synthesis of thiolated gold clusters longer ~~etching~~ ageing ?? times led to narrower size distribution, because only the most stables structures remained.

Following these directions, a pink product was obtained. In order to separate different cluster sizes, the sample was passed through a size exclusion chromatography column (SEC) [28-29], until a single fraction with characteristic and well-defined UV-Vis spectrum was obtained (as discussed below). The synthesis was repeated several times, each time reproducibly leading to the same highly stable product (dissolved in DCM or toluene). Once the sample was dried (powder form) and after some air exposure it got oxidized to an insoluble black precipitate.

Finally, a precise and reproducible synthesis route was developed, yielding for the first time stable thiolated cobalt clusters.

**Structure and Properties Characterization.** For studies of the composition of thiolated metal clusters, MALDI TOF mass spectrometry is the most frequently applied technique. In the case of Au clusters, *trans*-2-[3-(4-*tert*-butylphenyl)-2-methyl-2-propenylicene] malanonitrile (DCTB) was found as an optimal matrix, with a low degree of metal cluster fragmentationFor cobalt clusters using a DCTB matrix led to a higher degree of fragmentation in the low m/z range, even under lower laser irradiance, similar as observed before for thiolated iridium clusters.[14] After screening different matrices, 2,4,6-trihydroxyacetophenone (THAP) lead to a lower degree of fragmentation and reproducible results for the synthesized thiolated cobalt clusters. Figure 1 shows the MALDI TOF mass spectrum obtained from $Co_x(SC_2H_4Ph)_m$ in ion positive mode. The analysis of the mass spectrum revealed a difference of m/z=334 between the major peaks, which corresponds to the oligomer $Co(SR)_2$ unit (monometallic staple). The same type of characteristic fragment was also observed in MALDI mass spectra of thiolated gold clusters. The range of observed masses was between m/z=1826 and m/z=3968; the higher one seems related to clusters containing $Co_{30}(SR)_{16}$, but due to the high degree of fragmentation it was not possible to assign a specific formula. The MALDI MS results suggest formation of cobalt clusters in a range of 25-30 cobalt atoms, with a clear fragmentation pattern of staple motifs (-S-Co-S-), which are characteristic of thiolate protected metal clusters. Several groups, such as Tsukuda, Dass, Murray or McLean, have analyzed thiolated protected clusters by MADI and ESI-MS, reporting this kind of staple fragmentation, related with the direct desorbing process of the capping structures from the AuNP surface. [30] [31-36]

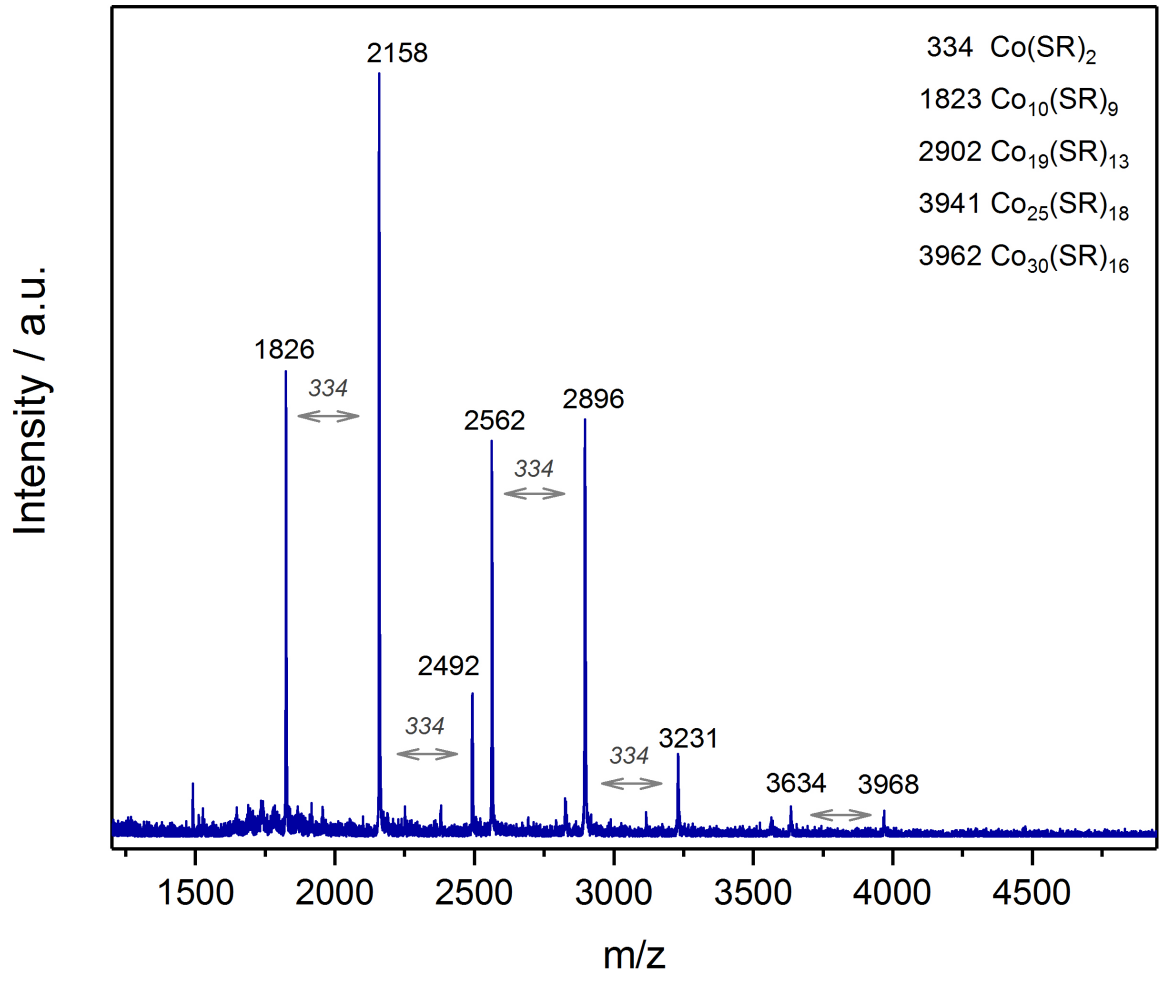


**Figure 1**. MALDI-TOF spectra of the prepared $Co_x(SR)_m$ clusters.

In order to obtain complementary insight on cluster composition, thermogravimetric analysis (TGA) was performed. The TGA profile (Figure S1 Supporting Information) shows a weight loss of 59% between 75C and 375C that is related to the removal of the thiolate ligands ($-SC_2H_4Ph$). The higher range of m/z observed by MALDI-MS, i.e. $Co_{25}(SR)_{18}$ and $Co_{30}(SR)_{16}$ clusters, would exhibit a weight loss related to ligands of 62% and 55%, respectively. Thus, the 59% weight loss observed for the synthesized cobalt clusters is in good agreement with that expected

from the cobalt cluster compositions determined by MALDI. However, three steps were observed during the ligand removal process; weight losses of 8% at lower temperature (75°C-150°C), a main weight loss of 41% at 150°C-275°C, and 10% loss at higher (275°C-375°C) temperature.Previous studies on thiolated gold clusters have also reported different weight loss steps that were ascribed to different staple configurations (long and short staples), but also to the interaction of the oxidative atmosphere with thiol ligands, that may lead to different removal processes. These may explain the two higher temperature steps for cobalt clusters. Carotenuto *et al.* studied the thermal stability of cobalt thiolates (Co-$C_{18}H_{37}SH$) and also reported two weight losses at 260°C and 360°C. [16] Thus, the low temperature step may be due to oxide species attached to the clusters (cf. FTIR and XPS below).

X-ray diffraction measurements were performed to confirm the formation of Co clusters and to discard $CoS_x$ complexes or Co nanoparticles, which exhibit highly crystalline structures, as reported in literature.[16, 37-38] XRD revealed that our samples were not crystalline (Figure S2 Supporting Information).

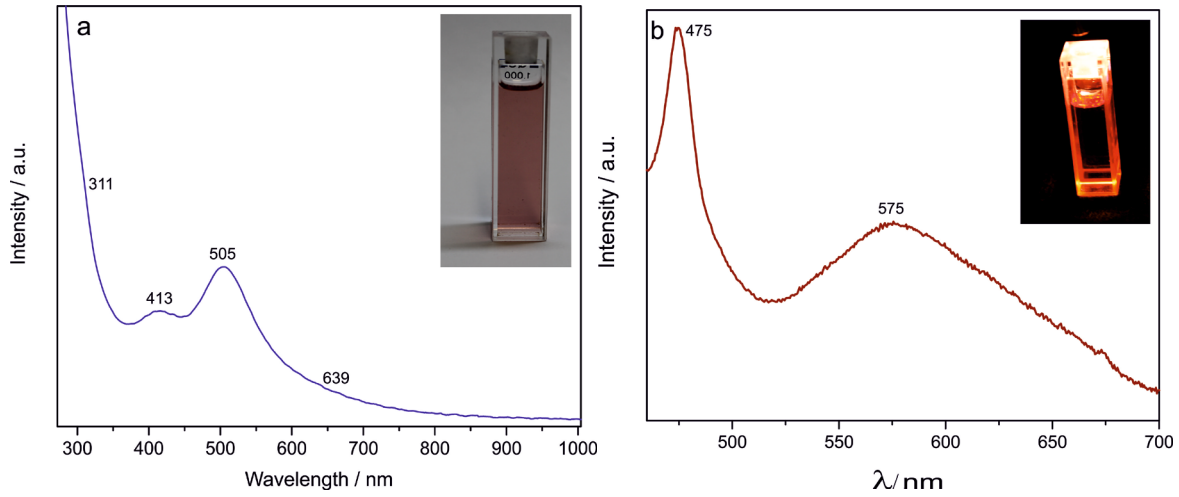

**Figure 2.** (a) UV-Vis absorption spectrum; (b) Photoluminescence spectrum; inside photographs of the cobalt cluster dichloromethane solution are shown as insets, without and with UV-Vis illumination (λ from 220-400nm).

Due to their molecule-like electronic structure, atomic scale metal nanoclusters exhibit one or more absorption peaks in UV-Vis, in contrast to the surface plasmon resonance (SPR) band observed for larger particles. UV-Vis absorption spectra of the synthesized cobalt clusters dissolved in dichloromethane (DCM) (Fig. 2a) exhibit four main absorption peaks, at 311, 413, 506 and 639 nm. A comparison with the characteristic SPR band of larger Co nanoparticles is not straightforward due to conflicting reports in literature. Based on Mie's theory calculations and experimental studies very weak absorption is expected in the range of 250–450 nm (285nm [39], 360nm and 495nm[40]) and in the range of 497-520nm[17] (520 nm[41]), but all reports agree that SPR is represented by a very broad band. Thus, the formation of clusters is evidenced by the defined (and not broad) absorption bands at different wavelengths. In order to compare the cobalt clusters with common cobalt nanoparticles, the latter were prepared according to reported methods,[16-17] with an additional passivation step with the same thiolated ligand ($SC_2H_4Ph$). The particles are stable only for short time and form an un-soluble black precipitate. Nevertheless, a comparison of UV-Vis spectra of short living cobalt nanoparticles in DCM with Cox(SR)m clusters is shown in Figure S3. For nanoparticles, the bands are broader and shifted..

Figure 2(b) shows the photoluminescence spectrum of the cobalt clusters. The emission spectrum upon excitation at 413nm shows intense luminescence peaks at the blue and yellow region, with two emission peaks at 475nm and 575nm. The observed dual fluorescence is a typical indicator of charge transfer occurring in the clusters upon excitation. Previous studies on

glutathione-protected gold clusters also displayed such dual luminescence,[42-44] which was explained by Whetten *et al.*: the high energy luminescence being an inter-band transition from excited states in the sp-band to the d-band,[45] and the low energy as the intraband HOMO-LUMO transition within the sp band. However, complementary calculations and studies would be required to explain the origin of the dual luminescence of cobalt clusters.

STEM images showed uniform cobalt clusters with an average particle size around 2 nm, as displayed in Figure 3. EELS analysis at the Co L3 edge indicated a tendency of the Co L3 edge to shift to lower energies for the center of the cluster, and to higher energies at the cluster edge, which would point to metallic Co at the center and an oxidized perimeter (that may be due to oxidation upon deposition on the TEM grid; Fig. S4 Supporting Information).[46-47] The onset and shape of the Co L3 edge of the sum spectrum acquired at the center of the cluster indicated metallic Co atoms,[46, 48] in agreement with the selected area electron diffraction (SAED) pattern (Fig. S4).

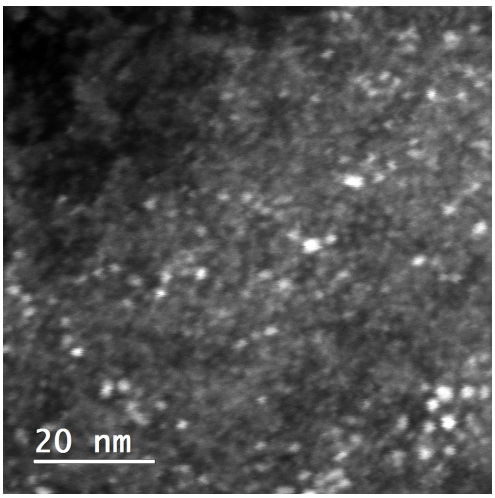


Figure 3. STEM image of the $Co_x(SR)_m$ clusters.

In order to corroborate the structure and size information, room temperature STM measurements were performed. Figure 4 shows clusters with roughly spherical shape, deposited on highly

ordered pyrolytic graphite (HOPG). HOPG was chosen as substrate surface as it is atomically flat and clean, which facilitates the detection of nanoclusters and reliable measurements of cluster size and height. Cluster size analysis via line profiles indicated an average size of 1.3 nm and 1 nm height (see Figure S5 Supporting Information). Atomically resolution of the clusters was not obtained, likely due to the insulating character of the ligands and the sample temperature of 300 K.

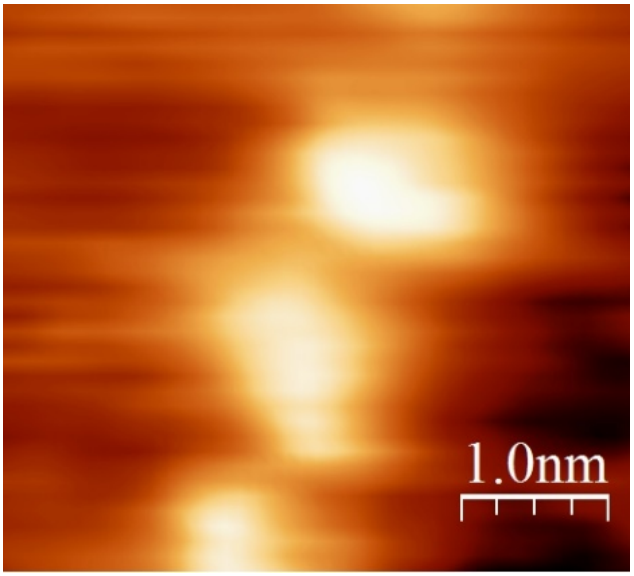


**Figure 4**. STM image of Co clusters supported on HOPG, taken at room temperature ($V_{sample}$ = +1.6 V, $I_{tunnel}$ = 0.35 nA). The cluster size is ~1.3 nm.

Vibrational Spectroscopy is a useful technique for studying molecular conformation and nanomaterials properties. The Raman spectrum of the synthesized $Co_x(SR)_m$ clusters (Figure 5a) in the range of 200-2000 $cm^{-1}$ shows characteristic peaks at higher energies, an intense peak at 1100$cm^{-1}$ related to the bonded thiolated ligands ($-SC_2H_4Ph$), and another around 1420 $cm^{-1}$ related to the aromatic ring. Based on previous Raman studies of metal sulfides, the peaks between 200 - 450 $cm^{-1}$ can be attributed to Co-S vibrations, with a prominent band around 350 $cm^{-1}$.[18] Figure 5b displays a spectrum of the $Co_x(SR)_y$ clusters at low wavenumber region, with a

broad peak at 322cm$^{-1}$ and smaller one at 419 cm$^{-1}$, assigned to Co-S vibrations in agreement with previous studies.[18, 49-51] The comparison of Raman spectra of the prepared $Co_x(SR)_m$ clusters with those reported for different $CoS_x$ compounds (nanostructures, complexes…) revealed pronounced differences of the vibrational bands (Raman shifts) and relative intensities. However, when the Raman spectra of cobalt clusters are compared those of monolayer protected thiolated metal clusters several similarities are apparent.[52-55] Thiol ligands in similar environments or configurations (like staples) should exhibit similar vibrational properties for Co and Au, but the frequencies may be slightly shifted due to different masses and force constants.

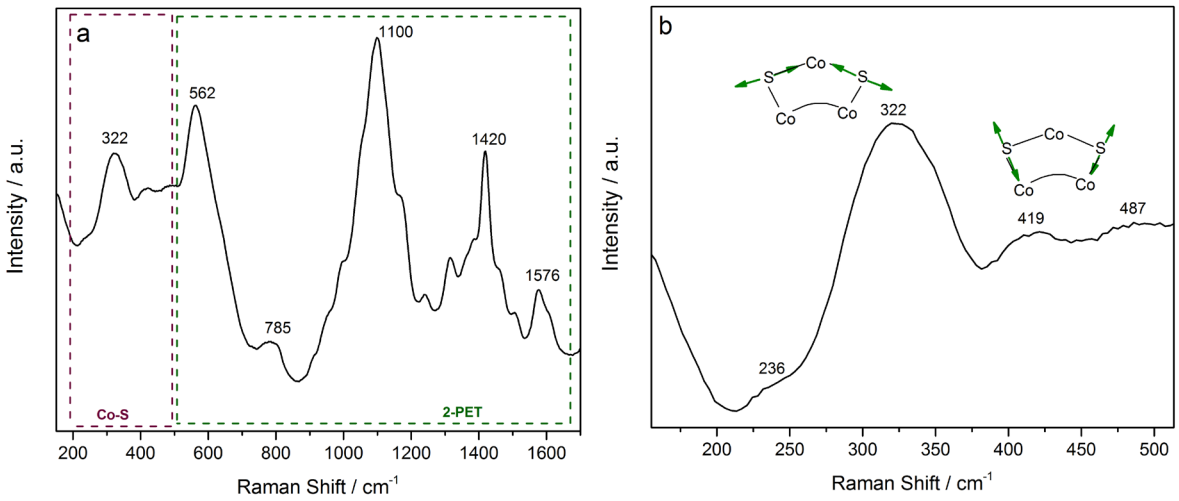


**Figure 5.** Raman spectra of $Co_x(SR)_m$ clusters.

Raman spectroscopy of gold clusters have focused on the Au-S interface and both experimental and theoretical studies were reported.[56-59] Two types of Au-S stretching vibrations can be distinguished at lower wavenumber range (200-350 cm$^{-1}$), related to Au(core)-S (radial mode) and to Au(staple)-S (tangential mode) bonds. Different radial vibrations were observed depending on the type of staples: whereas short staples lead to vibrations at lower energies, the bending of longer staples requires higher energy.

The Co-S vibrational band is again expected to be shifted with respect to Au-S, based on the smaller mass of Co (Au is heavier), which should lead to a high frequency shift . However, the binding strength in Co-S is weaker than in Au-S, leading to a shift to lower frequency. In total, the two effects compensate each other and the Co-S band and Au-S band are similar. According to Raman studies of the Au-S vibration related to the staple configuration,[57] the presence of a single strong peak at 322cm$^{-1}$ can be attributed to the Co-S bond in the short staples, in agreement with the fragmentation pattern observed by MALDI-MS. The radial mode vibrations were reported for higher energies with low intensity (due to the movement of the thiolate against the cluster surface), and the small peaks between 400 and 500cm$^{-1}$ may thus be assigned to the Co(core)-S bonds.

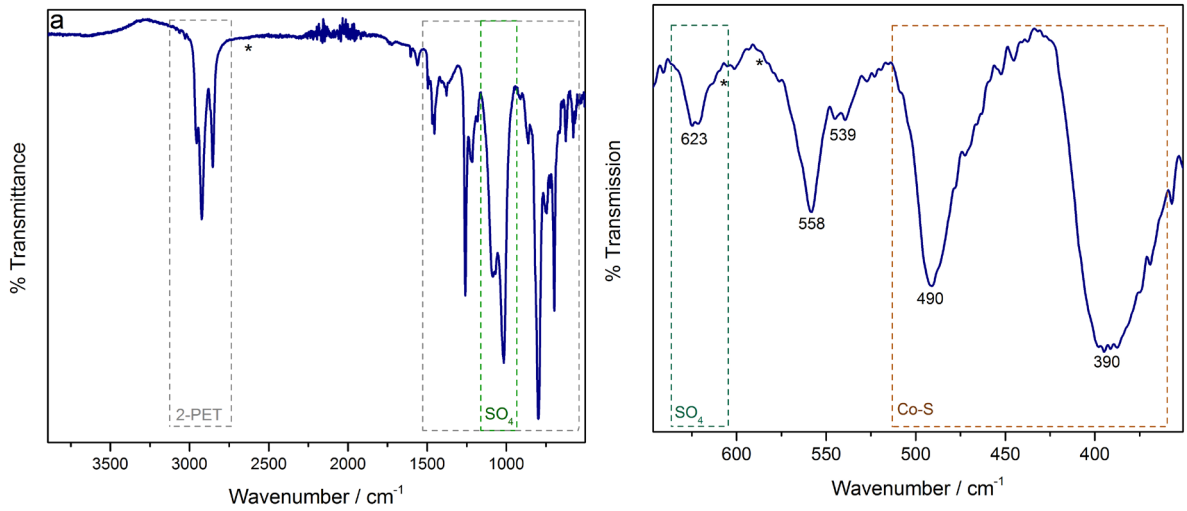


**Figure 6.** (a) MIR and (b) FIR FTIR spectra of $Co_x(SR)_m$ clusters.

For further structural characterization mid- and far-infrared FTIR measurements were performed. The bonding between Co and S is confirmed by the absence of the S-H stretching vibration, expected around 2525 cm$^{-1}$ in MIR spectra (Figure 6(a) marked by an *), whereas the

characteristic C-H, C-S and aromatic stretching bands of the $PhCH_2CH_2S$- ligand were indeed observed. In addition, the spectrum shows an unexpected strong band at 1000-1200 $cm^{-1}$. Based on literature, S=O stretching bands of sulfur oxide compounds produce strong infrared bands in the 1400–1000 $cm^{-1}$ range. Figure 6(b) shows the FIR region, also displaying a band at 623 $cm^{-1}$ that may be assigned to the asymmetric bending of the $SO_4$ groups, typically found between 600 and 640 $cm^{-1}$. Thus, the bands observed in the MIR spectra confirm the presence of sulfur oxide species. The band around 550$cm^{-1}$ is related to mercaptan compounds, in this case the thiol ligand. The bands observed between 350 and 500 $cm^{-1}$ further confirm the Co-S bond.

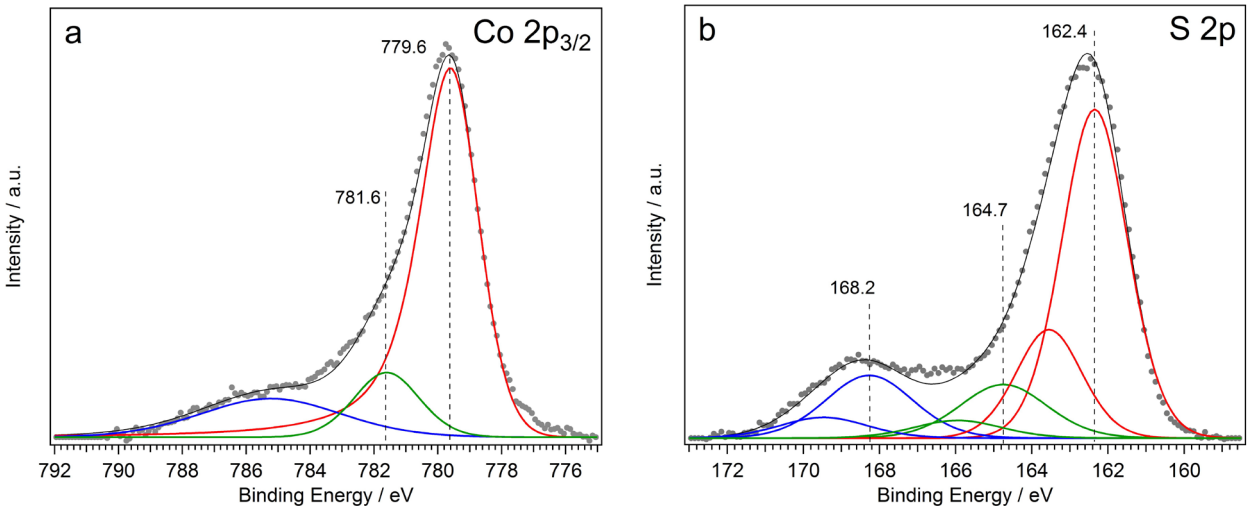


**Figure 7**. XPS spectra of (a) the Co $2p_{3/2}$ and (b) the S $2p_{3/2}$ and S $2p_{1/2}$ core level shifts of the $Co_x(SR)_m$ clusters on HOPG.

XPS analysis was performed to determine the valence state of the cobalt clusters. Figure 7a shows the Co $2p_{3/2}$ region, including peak fitting. The 779.6 eV signal is attributed to metallic cobalt from the clusters. Similarly to monolayer protected Au-clusters the binding energy Co-clusters is 1.5 eV higher than bulk metallic Co.[60] Zhang showed for decreasing size of AuSR nanoparticles, that the Au 4f peaks shift to higher binding energy.[61] This shift results from a nanosize effect and from surface metal−ligand interactions in the nanoparticles.[61] The signal at 781.6 eV can be attributed either to the cobalt-sulfur bond or to cobalt oxide (CoO). The observed plasmon feature at ~785 eV fits both Co-S and CoO. In comparison, $Co_3O_4$ is missing the plasmon feature.[62] Tao et al. and Ganesan et al. reported BEs of 781.4 and 781.3 eV for, cobalt sulfide nanoparticles, respectively.[38, 63] Due to the nanosize effect also the BE of CoO may be shifted by 1.5 eV to higher BE. An unambiguous assignment of the 781.6 eV feature to either Co-S or CoO would require additional high-resolution measurements, however. Although, the additional results from SAED, Raman or XAFS indicate the Co-S bonds rather than CoO.

In the S 2p spectra (Fig. 7b), the signal comprises three components, at 162.4 eV, 164.7 eV and 168.2 eV. As this is the first report of synthesis of protected cobalt clusters, there are no reference data but studies of self-assembled monolayers (SAM) of metallic cobalt provide useful results for S2p. The peak at 162.4 eV can be attributed to the sulfur-cobalt bond, in agreement with values for S-Co - of SAMs (~162,5 eV, dodecanethiol), reported by Devillers et al. [64]and (162.8 eV, octadecanethiol) by Pookpanratana et al. .[65] The peak at 168.2 eV can be attributed to fully oxidized sulfur. Once more, this agrees with the results of Devillers et al. which reported oxidation of sulfur (~168.5 eV) in the SAMs, when the surface was not fully covered and oxygen reacted with the SAM. Similarly, Pookpanratana et al. reported fully oxidized sulfur at

~168.6 eV. Further, partly oxidized sulfur is present, corresponding to the S2p signal at 164.7 eV.[66]

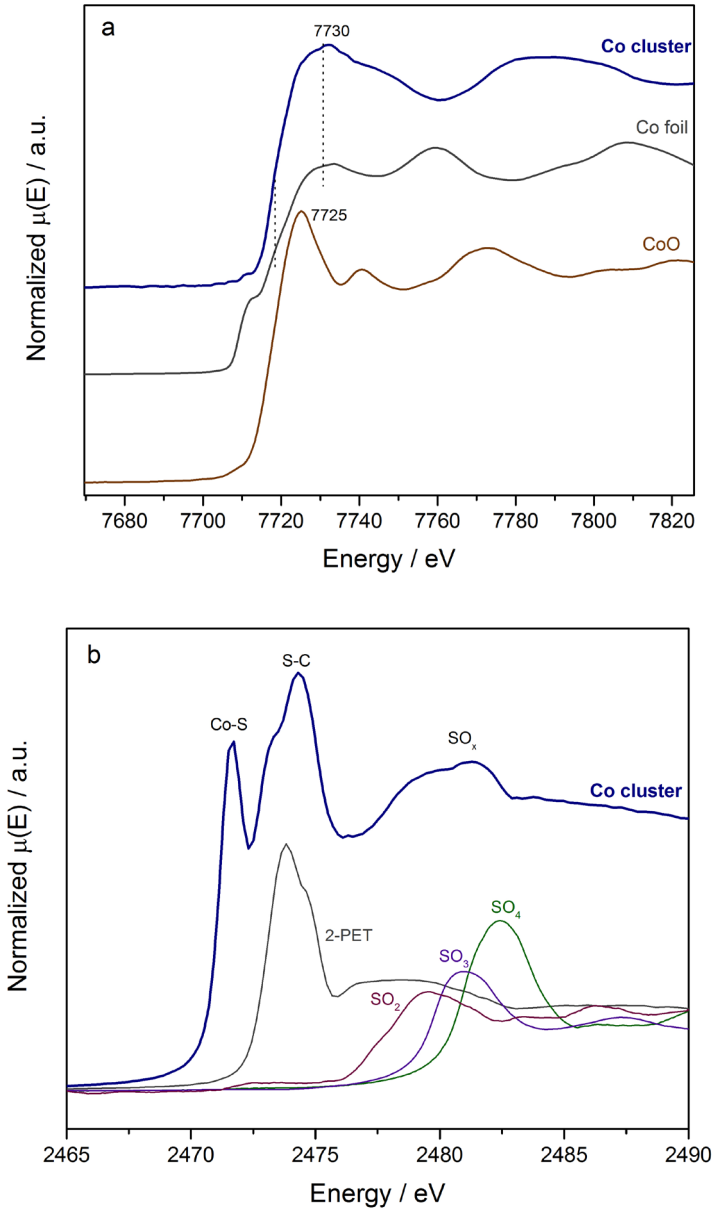


**Figure 8.** XANES spectra at the Co K-edge (a) and S K-edge (b) of the $Co_x(SR)_m$ clusters and reference materials.

The electronic structure and the local chemical environment of the $Co_x(SR)_m$ clusters were studied by X-ray absorption near edge spectroscopy (XANES) at the Co K-edge (Fig. 8a) and S K-edge (Fig. 8b) and compared to reference samples: Co foil, CoO, thiol ligand(2-PET), $SO_2$, $SO_3$ and $SO_4$ . In case of Co K-edge XANES spectra, the high intensity of the white line, the edge position and the broad white line feature for $Co_x(SR)_m$ clusters – when compared to the reference materials - suggest the presence of Co-S bonds[18] in the cluster structure (Fig. 8a). In the case of S K-edge XANES, the reference samples indicate that the white line intensity decrease and the edge position energy increase with increasing sulfur oxidation, changing from 2471 eV for $S^{-2}$ to 2483 eV for $S^{6+}$. From the peak positions in S K-edge XANES of $Co_x(SR)_m$ clusters three kinds of sulfur states can be distinguished: a first one at 2471eV, corresponding to an approximated oxidation state of -1, a second one at 2479-2481 eV related to oxidized ($SO_x$) sulfur species, and a third one at 2474eV corresponding to the S-C bond of the thiolate ligand. The Co-S bond was already observed by Raman and FTIR (Fig. 5 and Fig. 6), and is confirmed by Co and S K-edge XANES.

## CONCLUSIONS

We report the first successful synthesis of monolayer protected thiolate cobalt clusters is. Due to cluster fragmentation, their exact molecular mass and/or distribution could not be determined by MALD-MS. However, taking into account the complementary TG analysis, a cluster size in the range of 25-30 cobalt atoms is expected. This is confirmed by STEM and STM images showing uniform clusters of approximately 2 nm size. The MALDI-MS results also revealed a uniform fragment, corresponding to a monomeric staple unit (-S-Co-S-), which was corroborated

by Raman. Furthermore, XPS, XAFS and EELS analysis indicated a metallic state of cobalt. The different characterization results point to characteristic structural features and properties of thiolate protected Co clusters. The cobalt clusters were stable in solution, but upon air contact of the dry powder state it oxidized and decomposed to a black powder that was insoluble in almost any solvent. XPS analysis together with XANES and FTIR revealed the presence of oxidized sulfur (with two different kinds of sulfur species), which protects the metallic oxidation state of cobalt. Based on the current synthesis and the characterization results, more detailed studies of the exact Co cluster size, composition and physical/chemical properties are to be performed in the near future.

ASSOCIATED CONTENT

**Supporting Information**.

Complementary pictures of Thermogravimetric analysis; X-ray Diffraction pattern; UV-Vis spectra; HAADF, EDX and EELS from STEM studies; and additional STM images with the line profiles of the cobalt clusters.

The authors declare no competing financial interest.

AUTHOR INFORMATION

**Corresponding Author**

*Noelia Barrabés: E-mail: noe.barrabes@gmail.com; Noelia.rabanal@tuwien.ac.at ;

Tel: +43(1) 58801 165 109

**Notes**

The authors declare no competing financial interest

**Author Contributions**

The manuscript was written through contributions of all authors. All authors have given approval to the final version of the manuscript.

**ACKNOWLEDGMENT**

This work was supported by the Austrian Science Fund (FWF) through the international DACH program I 1041-N28 (COMCAT) and through project SFB FOXSI (F4502-N16). Beamtime Proposal (20155134) granted at Ellectra Synchrotron. We thank the Swiss Light Source for granting beamtime at the SuperXAS beamline. We grateful to Bei Zhang, Annelies Seels and Giovanni Salassa from University of Geneva for the help in the XAS measurements; Philipp Baloh from TU-Wien for Raman measurements and Prof. Thomas Bürgi for helpful discussions.

**REFERENCES**

1. Tsukuda, T.; Häkkinen, H., *Protected Metal Clusters: From Fundamentals to Applications*; Elsevier, 2015; Vol. 9.
2. Jin, R.; Zeng, C.; Zhou, M.; Chen, Y., Atomically Precise Colloidal Metal Nanoclusters and Nanoparticles: Fundamentals and Opportunities. *Chem. Rev.* **2016**, *116*, 10346-10413.
3. Lu, Y.; Chen, W., Sub-Nanometre Sized Metal Clusters: From Synthetic Challenges to the Unique Property Discoveries. *Chem. Soc. Rev.* **2012**, *41*, 3594-3623.
4. Jin, R., Atomically Precise Metal Nanoclusters: Stable Sizes and Optical Properties. *Nanoscale* **2015**, *7*, 1549-1565.
5. Wu, Z. K.; Wang, M.; Yang, J.; Zheng, X. H.; Cai, W. P.; Meng, G. W.; Qian, H. F.; Wang, H. M.; Jin, R. C., Well-Defined Nanoclusters as Fluorescent Nanosensors: A Case Study on Au25(Sg)18. *Small* **2012**, *8*, 2028-2035.
6. Yoshimoto, J.; Sangsuwan, A.; Osaka, I.; Yamashita, K.; Iwasaki, Y.; Inada, M.; Arakawa, R.; Kawasaki, H., Optical Properties of 2-Methacryloyloxyethyl Phosphorylcholine-

Protected Au4 Nanoclusters and Their Fluorescence Sensing of C-Reactive Protein. *J. Phys. Chem. C* **2015**, *119*, 14319-14325.
7. Luo, Z.; Zheng, K.; Xie, J., Engineering Ultrasmall Water-Soluble Gold and Silver Nanoclusters for Biomedical Applications. *Chem. Commun.* **2014**, *50*, 5143-5155.
8. Zhu, Y.; Qian, H. F.; Jin, R. C., Catalysis Opportunities of Atomically Precise Gold Nanoclusters. *J. Mater. Chem.* **2011**, *21*, 6793-6799.
9. Yamazoe, S.; Koyasu, K.; Tsukuda, T., Nonscalable Oxidation Catalysis of Gold Clusters. *Acc. Chem. Res.* **2014**, *47*, 816-824.
10. Ji, J.; Wang, G.; Wang, T.; You, X.; Xu, X., Thiolate-Protected Ni39 and Ni41 Nanoclusters: Synthesis, Self-Assembly and Magnetic Properties. *Nanoscale* **2014**, *6*, 9185-9191.
11. Kagalwala, H. N.; Gottlieb, E.; Li, G.; Li, T.; Jin, R. C.; Bernhard, S., Photocatalytic Hydrogen Generation System Using a Nickel-Thiolate Hexameric Cluster. *Inorg. Chem.* **2013**, *52*, 9094-9101.
12. Zhu, M.; Zhou, S.; Yao, C.; Liao, L.; Wu, Z., Reduction-Resistant and Reduction-Catalytic Double-Crown Nickel Nanoclusters. *Nanoscale* **2014**, *6*, 14195-14199.
13. Ganguly, A.; Chakraborty, I.; Udayabhaskararao, T.; Pradeep, T., A Copper Cluster Protected with Phenylethanethiol. *J. Nanopart. Res.* **2013**, *15*, 1522.
14. Bhat, S.; Chakraborty, I.; Maark, T. A.; Mitra, A.; De, G.; Pradeep, T., Atomically Precise and Monolayer Protected Iridium Clusters in Solution. *RSC Advances* **2016**, *6*, 26679-26688.
15. Puntes, V. F.; Krishnan, K. M.; Alivisatos, A. P., Colloidal Nanocrystal Shape and Size Control: The Case of Cobalt. *Science* **2001**, *291*, 2115-2117.
16. Carotenuto, G.; Pasquini, L.; Milella, E.; Pentimalli, M.; Lamanna, R.; Nicolais, L., Preparation and Characterization of Cobalt-Based Nanostructured Materials. *Eur. Phys. J. B* **2003**, *31*, 545-551.
17. Sanghamitra, N. J. M.; Mazumdar, S., Effect of Polar Solvents on the Optical Properties of Water-Dispersible Thiol-Capped Cobalt Nanoparticles. *Langmuir* **2008**, *24*, 3439-3445.
18. Kornienko, N.; Resasco, J.; Becknell, N.; Jian, C. M.; Liu, Y. S.; Nie, K. Q.; Sun, X. H.; Guo, J. H.; Leone, S. R.; Yang, P. D., Operando Spectroscopic Analysis of an Amorphous Cobalt Sulfide Hydrogen Evolution Electrocatalyst. *J. Am. Chem. Soc.* **2015**, *137*, 7448-7455.
19. Zhu, W. X.; Yue, X. Y.; Zhang, W. T.; Yu, S. X.; Zhang, Y. H.; Wang, J.; Wang, J. L., Nickel Sulfide Microsphere Film on Ni Foam as an Efficient Bifunctional Electrocatalyst for Overall Water Splitting. *Chem. Commun.* **2016**, *52*, 1486-1489.
20. Chen, C. J.; Chen, P. T.; Basu, M.; Yang, K. C.; Lu, Y. R.; Dong, C. L.; Ma, C. G.; Shen, C. C.; Hu, S. F.; Liu, R. S., An Integrated Cobalt Disulfide (Cos2) Co-Catalyst Passivation Layer on Silicon Microwires for Photoelectrochemical Hydrogen Evolution. *J Mater Chem A* **2015**, *3*, 23466-23476.
21. Zhao, X. Y.; Yang, Y.; Li, Y. H.; Cui, X.; Zhang, Y. H.; Xiao, P., Nico-Selenide as a Novel Catalyst for Water Oxidation. *J Mater Sci* **2016**, *51*, 3724-3734.
22. Sun, Z. J.; Lv, B. H.; Li, J. S.; Xiao, M.; Wang, X. Y.; Du, P. W., Core-Shell Amorphous Cobalt Phosphide/Cadmium Sulfide Semiconductor Nanorods for Exceptional Photocatalytic Hydrogen Production under Visible Light. *J Mater Chem A* **2016**, *4*, 1598-1602.
23. Huang, Z. F.; Song, J. J.; Li, K.; Tahir, M.; Wang, Y. T.; Pan, L.; Wang, L.; Zhang, X. W.; Zou, J. J., Hollow Cobalt-Based Bimetallic Sulfide Polyhedra for Efficient All-Ph-Value

Electrochemical and Photocatalytic Hydrogen Evolution. *J. Am. Chem. Soc.* **2016**, *138*, 1359-1365.
24. Iablokov, V.; Barbosa, R.; Pollefeyt, G.; Van Driessche, I.; Chenakin, S.; Kruse, N., Catalytic Co Oxidation over Well-Defined Cobalt Oxide Nanoparticles: Size-Reactivity Correlation. *ACS Catal.* **2015**, *5*, 5714-5718.
25. Brust, M.; Walker, M.; Bethell, D.; Schiffrin, D. J.; Whyman, R., Synthesis of Thiol-Derivatised Gold Nanoparticles in a Two-Phase Liquid-Liquid System. *J. Chem. Soc., Chem. Commun.* **1994**, 801-802.
26. Ravel, B.; Newville, M., Athena, Artemis, Hephaestus: Data Analysis for X-Ray Absorption Spectroscopy Using Ifeffit. *J. Synchrotron Radiat.* **2005**, *12*, 537-541.
27. Kern, R. J., Tetrahydrofuran Complexes of Transition Metal Chlorides. *J. Inorg. Nucl. Chem.* **1962**, *24*, 1105-1109.
28. Knoppe, S.; Boudon, J.; Dolamic, I.; Dass, A.; Burgi, T., Size Exclusion Chromatography for Semipreparative Scale Separation of Au-38(Sr)(24) and Au-40(Sr)(24) and Larger Clusters. *Anal. Chem.* **2011**, *83*, 5056-5061.
29. Barrabes, N.; Zhang, B.; Burgi, T., Racemization of Chiral Pd2au36(Sc2h4ph)(24): Doping Increases the Flexibility of the Cluster Surface. *J. Am. Chem. Soc.* **2014**, *136*, 14361-14364.
30. Tsunoyama, R.; Tsunoyama, H.; Pannopard, P.; Limtrakul, J.; Tsukuda, T., Maldi Mass Analysis of 11 Kda Gold Clusters Protected by Octadecanethiolate Ligands. *J. Phys. Chem. C* **2010**, *114*, 16004-16009.
31. Tracy, J. B.; Crowe, M. C.; Parker, J. F.; Hampe, O.; Fields-Zinna, C. A.; Dass, A.; Murray, R. W., Electrospray Ionization Mass Spectrometry of Uniform and Mixed Monolayer Nanoparticles: Au-25[S(Ch2)(2)Ph](18) and Au-25[S(Ch2)(2)Ph](18-X)(Sr)(X). *J. Am. Chem. Soc.* **2007**, *129*, 16209-16215.
32. Fields-Zinna, C. A.; Crowe, M. C.; Dass, A.; Weaver, J. E. F.; Murray, R. W., Mass Spectrometry of Small Bimetal Monolayer-Protected Clusters. *Langmuir* **2009**, *25*, 7704-7710.
33. Dass, A.; Dubay, G. R.; Fields-Zinna, C. A.; Murray, R. W., Fab Mass Spectrometry of Au25(Sr)18 Nanoparticles. *Anal. Chem.* **2008**, *80*, 6845-6849.
34. Harkness, K. M.; Fenn, L. S.; Cliffel, D. E.; McLean, J. A., Surface Fragmentation of Complexes from Thiolate Protected Gold Nanoparticles by Ion Mobility-Mass Spectrometry. *Anal. Chem.* **2010**, *82*, 3061-3066.
35. Harkness, K. M.; Cliffel, D. E.; McLean, J. A., Characterization of Thiolate-Protected Gold Nanoparticles by Mass Spectrometry. *Analyst* **2010**, *135*, 868-874.
36. Angel, L. A.; Majors, L. T.; Dharmaratne, A. C.; Dass, A., Ion Mobility Mass Spectrometry of Au25(Sch2ch2ph)18 Nanoclusters. *ACS Nano* **2010**, *4*, 4691-4700.
37. Liu, W.; Hu, E.; Jiang, H.; Xiang, Y.; Weng, Z.; Li, M.; Fan, Q.; Yu, X.; Altman, E. I.; Wang, H., A Highly Active and Stable Hydrogen Evolution Catalyst Based on Pyrite-Structured Cobalt Phosphosulfide. *Nat. Commun.* **2016**, *7*, 10771.
38. Ganesan, P.; Prabu, M.; Sanetuntikul, J.; Shanmugam, S., Cobalt Sulfide Nanoparticles Grown on Nitrogen and Sulfur Codoped Graphene Oxide: An Efficient Electrocatalyst for Oxygen Reduction and Evolution Reactions. *ACS Catal.* **2015**, *5*, 3625-3637.
39. Yeshchenko, O.; Dmitruk, I.; Alexeenko, A.; Dmytruk, A.; Tinkov, V., Optical Properties of Sol–Gel Fabricated Co/Sio2 Nanocomposites. *Physica E: Low-dimensional Systems and Nanostructures* **2008**, *41*, 60-65.

40. Zhang, J.; Lan, C. Q., Nickel and Cobalt Nanoparticles Produced by Laser Ablation of Solids in Organic Solution. *Mater. Lett.* **2008**, *62*, 1521-1524.
41. Ganeev, R. A., Nonlinear Refraction and Nonlinear Absorption of Various Media. *Journal of Optics A: Pure and Applied Optics* **2005**, *7*, 717.
42. Wei, W.; Lu, Y.; Chen, W.; Chen, S., One-Pot Synthesis, Photoluminescence, and Electrocatalytic Properties of Subnanometer-Sized Copper Clusters. *J. Am. Chem. Soc.* **2011**, *133*, 2060-2063.
43. Link, S.; Beeby, A.; FitzGerald, S.; El-Sayed, M. A.; Schaaff, T. G.; Whetten, R. L., Visible to Infrared Luminescence from a 28-Atom Gold Cluster. *J. Phys. Chem. B* **2002**, *106*, 3410-3415.
44. Yam, V. W.-W.; Cheng, E. C.-C.; Zhou, Z.-Y., A Highly Soluble Luminescent Decanuclear Gold(I) Complex with a Propeller-Shaped Structure. *Angew. Chem. Int. Ed.* **2000**, *39*, 1683-1685.
45. Bigioni, T. P.; Whetten, R. L.; Dag, Ö., Near-Infrared Luminescence from Small Gold Nanocrystals. *J. Phys. Chem. B* **2000**, *104*, 6983-6986.
46. Ewels, P.; Sikora, T.; Serin, V.; Ewels, C. P.; Lajaunie, L., A Complete Overhaul of the Electron Energy-Loss Spectroscopy and X-Ray Absorption Spectroscopy Database: Eelsdb.Eu. *Microsc. Microanal.* **2016**, *22*, 717-724.
47. Zhao, Y.; Feltes, T. E.; Regalbuto, J. R.; Meyer, R. J.; Klie, R. F., In Situ Electron Energy Loss Spectroscopy Study of Metallic Co and Co Oxides. *J. Appl. Phys.* **2010**, *108*, 063704.
48. Taylor, A.; Floyd, R. W., Precision Measurements of Lattice Parameters of Non-Cubic Crystals. *Acta Crystallographica* **1950**, *3*, 285-289.
49. Lyapin, S. G.; Utyuzh, A. N.; Petrova, A. E.; Novikov, A. P.; Lograsso, T. A.; Stishov, S. M., Raman Studies of Nearly Half-Metallic Ferromagnetic Cos 2. *J. Phys.: Condens. Matter* **2014**, *26*, 396001.
50. Shadike, Z.; Cao, M.-H.; Ding, F.; Sang, L.; Fu, Z.-W., Improved Electrochemical Performance of Cos2-Mwcnt Nanocomposites for Sodium-Ion Batteries. *Chem. Commun.* **2015**, *51*, 10486-10489.
51. Anastassakis, E.; Perry, C. H., Light Scattering and Ir Measurements in Xs2 Pryite-Type Compounds. *The Journal of Chemical Physics* **1976**, *64*, 3604-3609.
52. Varnholt, B.; Oulevey, P.; Luber, S.; Kumara, C.; Dass, A.; Burgi, T., Structural Information on the Au-S Interface of Thiolate-Protected Gold Clusters: A Raman Spectroscopy Study. *J. Phys. Chem. C* **2014**, *118*, 9604-9611.
53. Burgi, T., Properties of the Gold-Sulphur Interface: From Self-Assembled Monolayers to Clusters. *Nanoscale* **2015**, *7*, 15553-15567.
54. Xue, Y.; Li, X.; Li, H.; Zhang, W., Quantifying Thiol–Gold Interactions Towards the Efficient Strength Control. *Nat. Commun.* **2014**, *5*, 4348.
55. Varnholt, B.; Guberman-Pfeffer, M. J.; Oulevey, P.; Antonello, S.; Dainese, T.; Gascón, J. A.; Bürgi, T.; Maran, F., Vibrational Coupling Modulation in N-Alkanethiolate Protected Au25(Sr)180 Clusters. *J. Phys. Chem. C* **2016**, *120*, 25378-25386.
56. Tlahuice-Flores, A., Ligand Effects on the Structure and Vibrational Properties of the Thiolated Au18 Cluster. *Progress in Natural Science: Materials International* **2016**, *26*, 510-515.
57. Varnholt, B.; Oulevey, P.; Luber, S.; Kumara, C.; Dass, A.; Bürgi, T., Structural Information on the Au–S Interface of Thiolate-Protected Gold Clusters: A Raman Spectroscopy Study. *J. Phys. Chem. C* **2014**, *118*, 9604-9611.

58. Tlahuice-Flores, A.; Whetten, R. L.; Jose-Yacaman, M., Vibrational Normal Modes of Small Thiolate-Protected Gold Clusters. *J. Phys. Chem. C* **2013**, *117*, 12191-12198.
59. Parker, J. F.; Choi, J.-P.; Wang, W.; Murray, R. W., Electron Self-Exchange Dynamics of the Nanoparticle Couple [Au25(Sc2ph)18]0/1− by Nuclear Magnetic Resonance Line-Broadening. *J. Phys. Chem. C* **2008**, *112*, 13976-13981.
60. Lukashuk, L., et al., Operando Xas and Nap-Xps Studies of Preferential Co Oxidation on Co3o4 and Ceo2-Co3o4 Catalysts. *J. Catal.* **2016**, *344*, 1-15.
61. Zhang, P., X-Ray Spectroscopy of Gold–Thiolate Nanoclusters. *J. Phys. Chem. C* **2014**, *118*, 25291-25299.
62. Ferstl, P., et al., Adsorption and Activation of Co on Co3o4(111) Thin Films. *J. Phys. Chem. C* **2015**, *119*, 16688-16699.
63. Tao, F.; Zhao, Y.-Q.; Zhang, G.-Q.; Li, H.-L., Electrochemical Characterization on Cobalt Sulfide for Electrochemical Supercapacitors. *Electrochem. Commun.* **2007**, *9*, 1282-1287.
64. Devillers, S.; Hennart, A.; Delhalle, J.; Mekhalif, Z., 1-Dodecanethiol Self-Assembled Monolayers on Cobalt. *Langmuir* **2011**, *27*, 14849-14860.
65. Pookpanratana, S.; Lydecker, L. K.; Richter, C. A.; Hacker, C. A., Self-Assembled Monolayers Impact Cobalt Interfacial Structure in Nanoelectronic Junctions. *J. Phys. Chem. C* **2015**, *119*, 6687-6695.
66. Lindberg, B. J.; Hamrin, K.; Johansson, G.; Gelius, U.; Fahlman, A.; Nordling, C.; Siegbahn, K., Molecular Spectroscopy by Means of Esca Ii. Sulfur Compounds. Correlation of Electron Binding Energy with Structure. *Phys. Scr.* **1970**, *1*, 286.

TOC Figure

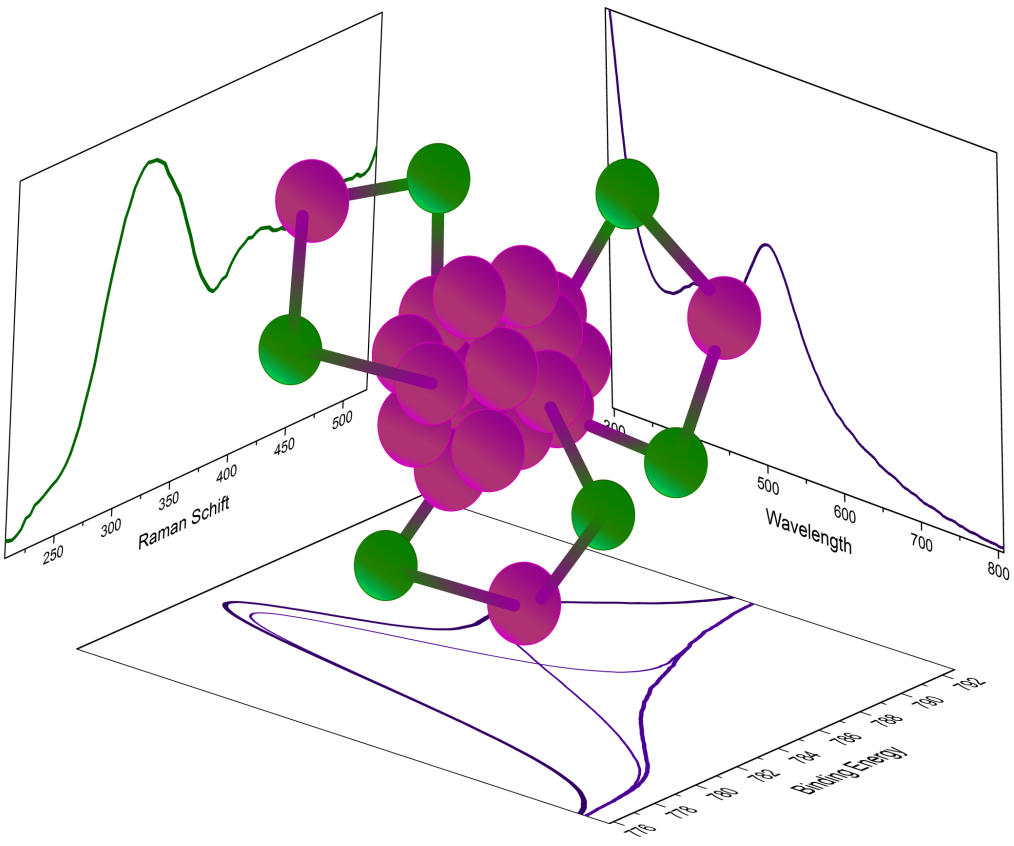
250
300
350
400
450
500
Raman Schift
500
600
700
800
Wavelength
776
778
780
782
784
786
788
790
792
Binding Energy